Metrol. Meas. Syst., Vol. 31 (2024) No. 4, pp. 797–812
DOI: 10.24425/mms.2024.152051

PAN POLSKA AKADEMIA NAUK

METROLOGY AND MEASUREMENT SYSTEMS
Index 330930, ISSN 0860-8229
www.metrology.wat.edu.pl

M&MS

$H\infty$ CONTROL AND EXPERIMENTAL STUDY OF MR SEMI-ACTIVE SUSPENSION WITH ACTUATOR RESPONSE DELAY

Renkai Ding[1,3)], Ping Wang[2)], Anze Li[3)], Ruochen Wang[4)], Dong Sun[4)], Ke Xu[5)]

1) State Key Laboratory of Automotive Simulation and Control, Jilin University, Changchun, Jilin 130015, China (✉ *drk@ujs.edu.cn*)
2) School of Communication Engineering, Jilin University, Changchun, Jilin 130015, China
3) Automotive Engineering Research Institute, Jiangsu University, Zhenjiang 212013, China
4) School of Automotive and Traffic Engineering, Jiangsu University, Zhenjiang 212013, China
5) Jiangsu Tangchen Automotive Parts Co., Ltd, Nantong 226500, China

Abstract

Given the potential negative impact of delayed response from a magnetorheological (MR) damper on the effectiveness of semi-active suspension (SAS), a specialized time-delay dependent H_∞ robust controller has been developed to address this issue. The controller accounts for the actuator response delay and determines the system theoretical critical delay. To mitigate the response delay within the electromagnetic loop of the actuator, a technique has been proposed and tested. The technique minimizes the overall response delay, ensuring it is less than the theoretical critical delay. Subsequently, feedback gain is determined and comparative performance tests are conducted to validate the efficacy of the proposed control method. Compared with a delay-independent H_∞ robust controller, it has been demonstrated that the body acceleration and dynamic tire load peak-to-peak responses generated by the proposed controller are decreased by 16.4% and 7.4% respectively under bumpy road conditions, while under stochastic road conditions, body acceleration decreases by 3.5%, suspension deflection by 17.1%, and DTL by 0.89%.

Keywords: Semi-active suspension, Actuator response delay, Time-delay dependent H_∞ robust controller, Theoretical critical delay, Comparative performance test.

1. Introduction

The magnetorheological *semi-active suspension* (SAS) dynamically adapts damping based on prevailing driving conditions, combining the universality and adaptability of active suspension [1–3] with low energy consumption. This has garnered significant attention and application [4]. However, time delay can have a negative impact on control effectiveness. If the controller design overlooks the delay issue, it may result in inconsistent output from the controller and input to the *magnetorheological* (MR) damper, rendering the feedback loop ineffective and degrading control performance. Furthermore, instability in the controlled object itself can

Article history: received May 15, 2025; revised July 31, 2024; accepted August 12, 2023; available online October 15, 2024.

lead to system instability. Although some literature [5] suggests that semi-active systems naturally exhibit stability and that issues related to time delay causing instability are unlikely, this viewpoint lacks rigor.

The delay of the magnetorheological SAS is mainly comprised of four aspects, as proposed in the literature [6]. The control force phase will demonstrate a specific overall time delay, encompassing the individual time delays of each component. Effectively managing the time delay of other components becomes challenging once the controller or actuator is designed, except the actuator response delay. Therefore, the primary focus in investigating time delays in SAS systems revolves around addressing response delays. Currently, there are two approaches to address the system response delay. One approach s Smith predictive control [7–9], while the other involves robust control based on the Lyapunov–Krasovskii stability theory [10–12]. The Smith predictive controller relies on an accurate mathematical model but. he presence of a model mismatch between the theoretical model and the actual device can result in poor closed-loop performance. The main idea of robust control based on the Lyapunov–Krasovskii stability theory is to construct a Lyapunov-Krasovskii functional or Lyapunov function and ensure its stability. In [13], Li developed a nonlinear system model that considers the time delay of the *continuous damping control* (CDC) system. The study focused on analysing the impact of the time delay on vehicle performance. In [14], Yang put forward a multi-objective optimization design for a time-delay feedback dynamic vibration absorber system with inertial stiffness. Through the optimization of both the system structure parameters and control parameters, effective control over the formant amplitude, anti-formant amplitude, and anti-resonance band symmetry of the main system was achieved. In [15], Liu proposed a comprehensive solution for analysing the variation pattern of critical instability time-delay in *inerter-spring-damper* (ISD) suspension. Based on the analysis findings, a method for selecting suspension parameters that can reduce the impact of the time delay is suggested. To improve the potential for energy harvesting and enhance the driving stability of nonlinear time-delay active suspension systems, Wu [16] introduced a time-delay active control technology. Moreover, in order to validate the effectiveness of the proposed method, a bench test was conducted using the dSPACE system. Zhu [17] proposed a delay-dependent sliding mode variable structure control method. To validate the actual performance, a real vehicle test was conducted. The conventional sliding mode controller and the Smith compensation controller were used for comparison during the test. The results demonstrated that the proposed controller outperformed the other two controllers. In order to investigate the potential and impact of the optimal time-delay feedback control, Nan [18] conducted a comparative experiment using active suspension equipment provided by Canada's Quanser Company. The experimental results indicate that, in comparison to LQR control, the proposed control method resulted in a 39.18% reduction in sprung mass acceleration under harmonic excitation and a 35.5% reduction under random road excitation.

To guarantee the system stability, designing a state feedback controller with time delay dependence is necessary, and making sure the system is stable by solving a given anti-jamming coefficient of critical delay, thus, the controller gain is obtained. However, the correlation between the theoretical critical delay and the actual response delay is often overlooked. Existing research frequently assumes that the response delay falls within the theoretical critical delay range, and then only verifies the rationality and effectiveness of the controller through simulation analysis. However, not all actuator response delays fall within the theoretical critical delay range. When the former exceeds the latter, it hinders effective controller gain acquisition. Additionally, different Lyapunov–Krasovskii generic functions will impact the design of the delay-dependent controller. Even with identical anti-interference coefficients, different delay-dependent controllers will have varying theoretical critical delays. Consequently, for a given actuator, one must consider the relationship between actual the response delay and the theoretical critical delay of the designed delay-dependent controller. Therefore, it is clear that existing assumptions are unreasonable.

Metrol. Meas. Syst., Vol. 31 (2024), No. 4, pp. 797–812
DOI: 10.24425/mms.2024.152051

The research is focused on the MR SAS system, with a specific emphasis on designing a time-delay dependent H∞ robust controller to address the actuator response delay. The theoretical critical delay is determined by specifying the anti-interference coefficient. Based on this, the actual actuator response delay is measured, and a method for reducing this delay is proposed to ensure that it falls within the theoretical critical time range. This, in turn, allows for obtaining the controller feedback gain.

The innovations outlined in this paper are as follows: the relationship between the actual response delay and the theoretical critical delay of the designed delay-dependent controller is considered. It is noted that existing researches usually assume that the actuator response delay falls within the theoretical critical delay range. Additionally, a method is put forward to minimize the response delay of the electromagnetic loop of the MR damper, thereby decreasing its overall response delay and ensuring that it remains less than the theoretical critical delay allowed by the controller.

2. MR SAS model

2.1. MR damper model

The Bingham model has the advantages of simple structure, clear physical meaning of parameters, and good engineering practicability and can be expressed as [19]:

$$\begin{cases} F(t) = c_e v(t) + F_{MR}(t)\,\mathrm{sgn}(v(t)) \\ F_{MR}(t) = a_4 I^4(t) + a_3 I^3(t) + a_2 I^2(t) + a_1 I(t) + a_0 \end{cases}, \tag{1}$$

where $F(t)$ represents the output control force; c_e represents the viscous damping coefficient; $v(t)$ denotes the motion velocity; $F_{MR}(t)$ represents the coulomb damping force; sgn$(\cdot)$ represents a symbolic function; Irepresents the control current; a_i $(i = 0, 1, 2, 3, 4)$ is the constant to be fitted.

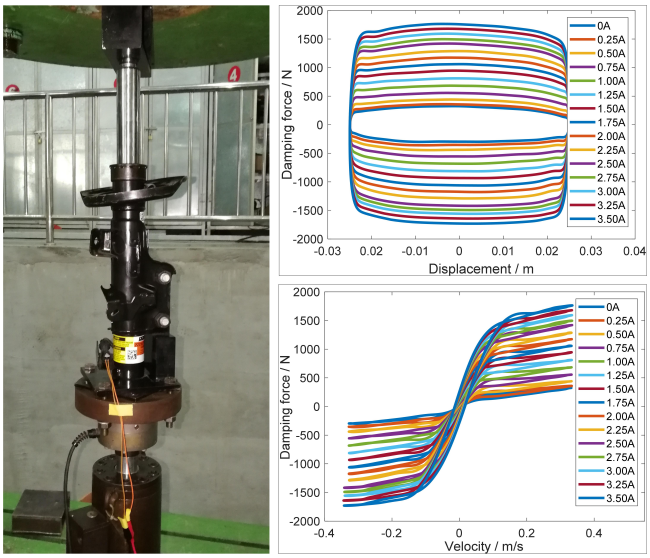

(a) test bench (b) test results

Fig. 1. Characteristic test.

In actuality, the controller calculates the control current based on the ideal control force in order to output the corresponding control force. Therefore, it is essential to use the current as the control quantity, establish a correlation between coulomb the damping force and the control current, and develop an inverse model. In this paper, the computing speed, fitting error and fitting effect of the system are considered comprehensively, and the relation is fitted as a first-order linear relation:

$$I(t) = b_1 F_{MR}(t) + b_0, \tag{2}$$

where b_0 andb_1 are constants to be fitted.

The maximum motion stroke is 90 mm, and the maximum input current is 3.5 A. The indicator diagram and speed characteristic curve measured by an INSTRON 8800 numerical control hydraulic servo vibration test bench (Fig. 1a) are shown in Fig. 1b. According to the test results, $c_e = 854.2$ N·s/m, $a_0 = 2.03$, $a_1 = 59.24$, $a_2 = 421.8$, $a_3 = -181.71$, $a_4 = 24.8$, $b_1 = -0.008248$, $b_2 = 0.002574$.

2.2. Response delay model

A 1/4 SAS model (Fig. 1) is established, and the system dynamics is as follows:

$$\begin{cases} m_s\ddot{x}_s(t) + c_e(\dot{x}_s(t) - \dot{x}_u(t)) + k_s(x_s(t) - x_u(t)) = u(t-\tau) \\ m_u\ddot{x}_u(t) - c_e(\dot{x}_s(t) - \dot{x}_u(t)) + c_t(\dot{x}_u(t) - \dot{x}_r(t)) - k_s(x_s(t) \\ -x_u(t)) + k_t(x_u(t) - x_r(t)) = -u(t-\tau) \end{cases}, \tag{3}$$

and

$$u(t-\tau) = \begin{cases} F_{MR}(t-\tau)\,\mathrm{sgn}(v(t)) & \text{if } F_{MR}(t-\tau)\,\mathrm{sgn}(v(t)) \cdot (v(t)) < 0 \\ 0 & \text{if } F_{MR}(t-\tau)\,\mathrm{sgn}(v(t)) \cdot (v(t)) \geq 0 \end{cases}, \tag{4}$$

where m_s and m_u represent sprung mass and unsprung mass, respectively, k_s and k_t represent spring stiffness and tire stiffness, respectively, c_t represents tire damping coefficient, x_s symbolizes the sprung mass stroke, x_t symbolizes the mass stroke, x_r represents road excitation, $u(t-\tau)$ represents the control input with variable time delay, τ represents the actuator response delay.

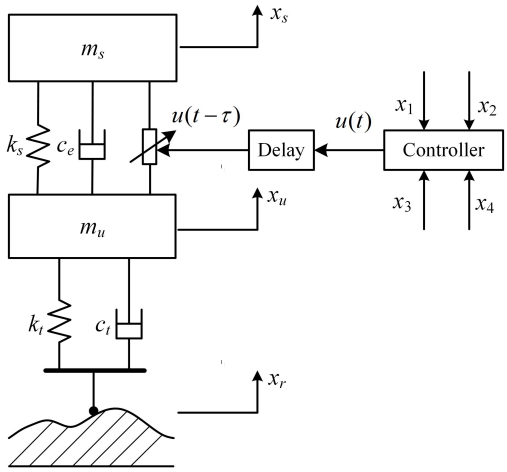

Fig. 2. MR SAS model.

Let

$$X(t) = [x_1(t),\ x_2(t),\ x_3(t),\ x_4(t)]^T, \quad Y(t) = [y_1(t),\ y_2(t),\ y_3(t)]^T,$$
$$Z(t) = [z_1(t),\ z_2(t),\ z_3(t),\ z_4(t)]^T, \quad U(t-\tau) = u(t-\tau), \quad W = \dot{x}_r(t).$$

and

$$x_1(t) = x_s(t) - x_u(t), \quad x_2(t) = x_u(t) - x_r(t), \quad x_3(t) = \dot{x}_s(t), \quad x_4(t) = \dot{x}_u(t),$$
$$y_1(t) = \ddot{x}_s(t), \quad y_2(t) = x_s(t) - x_u(t), \quad y_3(t) = x_u(t) - x_r(t),$$
$$z_1(t) = x_1(t), \quad z_2(t) = x_2(t), \quad z_3(t) = x_3(t), \quad z_4(t) = x_4(t),$$

$\dot{\boldsymbol{x}}_r(\boldsymbol{t})$ is road velocity input. Thus, the system equation can be obtained:

$$\begin{cases} \dot{X}(t) = AX(t) + BU(t-\tau) + EW(t) \\ Y(t) = CX(t) + DU(t-\tau) \\ Z(t) = GX(t) \end{cases},$$

$$A = \begin{bmatrix} 0 & 0 & 1 & -1 \\ 0 & 0 & 0 & 1 \\ -k_s/m_s & 0 & -c_e/m_s & c_e/m_s \\ k_s/m_u & -k_t/m_u & c_e/m_u & -(c_e+c_t)/m_u \end{bmatrix}, \quad B = \begin{bmatrix} 0 \\ 0 \\ 1/m_s \\ -1/m_u \end{bmatrix}, \tag{5}$$

$$E = \begin{bmatrix} 0 \\ -1 \\ 0 \\ c_t/m_u \end{bmatrix}, C = \begin{bmatrix} -k_s/m_s & 0 & -c_e/m_s & c_e/m_s \\ 1 & 0 & 0 & 0 \\ 0 & 1 & 0 & 0 \end{bmatrix}, \quad D = \begin{bmatrix} 1/m_s \\ 0 \\ 0 \end{bmatrix},$$

and G is the identity matrix.

The evaluation criteria are shown in (6) to (8), respectively [20].

$$\|A_{\text{acc}}\|_{\text{rms}} = \sqrt{\frac{1}{T}\int_0^T \|\ddot{x}_s\|^2\,\mathrm{d}t}, \tag{6}$$

$$\|F_{\text{dtl}}\|_{\text{rms}} = k_t\sqrt{\frac{1}{T}\int_0^T \|x_u - x_r\|^2\,\mathrm{d}t}, \tag{7}$$

$$\|f_{\text{sws}}\|_{\text{rms}} = \sqrt{\frac{1}{T}\int_0^T \|x_s - x_u\|^2\,\mathrm{d}t}, \tag{8}$$

where $\|A_{\text{acc}}\|_{\text{rms}}$ denotes the *root mean square* (RMS) of *body acceleration* (BA), which is commonly used to evaluate ride comfort; $\|F_{\text{dtl}}\|_{\text{rms}}$ denotes the RMS of the *dynamic tire load* (DTL), which is usually adapted to evaluate the handling performance; $\|f_{\text{sws}}\|_{\text{rms}}$ denotes the RMS of the *suspension deflection* (SD), which is usually used as s system constraint to evaluate the vehicle safety; T is the length of the sampled data.

3. Delay-dependent H_∞ robust controller

In order to design a time-delay dependent H_∞ robust controller for a SAS, it is necessary to develop a memoryless feedback control law based on (5) to meet the system performance criteria. The feedback control law can be expressed as follows:

$$U(t) = KX(t), \tag{9}$$

where K is the gain matrix of state feedback.

According to (5) and (9), the closed-loop system can be obtained:

$$\begin{cases} \dot{X}(t) = AX(t) + BKX(t) + EW(t) \\ Y(t) = CX(t) + DKX(t) \\ Z(t) = GX(t) \\ X(t) = \phi(t), \quad \forall t \in [-\tau, 0] \end{cases} \tag{10}$$

Under the condition of finite energy input signal $W(t) \in L_2[0, \infty)$, the closed-loop system shall meet the subsequent design specification:

(1) The closed-loop system is asymptotically stable;

(2) For a given anti-interference coefficient γ, in the case of zero initial value, it is required that the closed-loop system should be satisfied as $\|Y(t)\|_2 < \gamma\|W(t)\|_2$.

In order to mitigate the impact of actuator response delay on system control effectiveness, a Lyapunov–Krasovskii function is constructed:

$$V(t) = V_1(t) + V_2(t) + V_3(t), \tag{11}$$

where

$$V_1(t) = X^T(t)P_1X(t), \tag{12}$$

$$V_2(t) = \int_{-\tau}^{0}\int_{t+\beta}^{t} \dot{X}^T(\alpha)Z_2\dot{X}(\alpha)\,d\alpha\,d\beta, \tag{13}$$

$$V_3(t) = \int_{t-\tau}^{0}\int_{t+\beta}^{t} \dot{X}^T(\alpha)Q_1\dot{X}(\alpha)\,d\alpha\,d\beta. \tag{14}$$

The positive definite symmetric matrices P_1, Z_2 and Q_1 are to be solved, which is used to guarantee the negative definite of (11).

Assuming zero initial condition, that is for $\forall t \in [-\tau, 0]$ and $\phi(t) = 0$, there is $V(t)|_{t=0} = 0$. Next, the H_∞ performance of the system will be analysed, taking into consideration the following indicators:

$$J_{YW} = \int_0^\infty [Z^T(t)Z(t) - \gamma^2 W^T(t)W(t)]\,dt. \tag{15}$$

For all non-zero $W(t) \in L_2[0, \infty)$, if the negative definite of the Lyapunov–Krasovskii function (11) is guaranteed, we can further obtain:

$$\begin{aligned} J_{YW} &\le \int_0^\infty [Z^T(t)Z(t) - \gamma^2 W^T(t)W(t)]\,dt + V(t)|_{t=\infty} - V(t)|_{t=0} \\ &= \int_0^\infty [Z^T(t)Z(t) - \gamma^2 W^T(t)W(t) + \dot{V}(t)]\,dt = \int_0^\infty \eta T(t)\Pi\eta(t)\,dt, \end{aligned} \tag{16}$$

Metrol. Meas. Syst., Vol. 31 (2024), No. 4, pp. 797–812
DOI: 10.24425/mms.2024.152051

where

$$\eta(t) = [X(t), X(t-\tau), W(t)]^T,$$

$$\Pi = \begin{bmatrix} \Phi_1 & \Phi_2 & \tau A^T Z_2 E + P_1 E \\ \Phi_2^T & \Phi_3 & \tau K^T B^T Z_2 E \\ \tau E^T Z_2 A + E^T P_1 & \tau E^T Z_2 BK & -\gamma^2 I + \tau E^T Z_2 E \end{bmatrix},$$

$$\Phi_1 = A^T P_1 + P_1 A + \tau X_1 + Y_1 + Y_1^T + Q_1 + \tau A^T Z_2 A + C^T C,$$

$$\Phi_2 = P_1 BK - Y_1 + \tau A^T Z_2 BK + C^T DK,$$

$$\Phi_3 = -Q_1 + \tau K^T B^T Z_2 BK + K^T D^T DK.$$

Then the H_∞ performance $\|Y(t)\|_2 < \gamma \|W(t)\|_2$ can be achieved. Next, (16) can be analysed for its existence and stability conditions using the LMI method, while the critical delay of the system can be determined through conic complement linearization iteration. These methods enable the derivation and solution of key properties related to the equation and system in a rigorous and systematic manner. In this paper, a conical complement linearization iterative algorithm [21] is adopted to solve the problem, and the dichotomy method [22] on the basis of a given anti-interference coefficient γ is used to solve critical delay $\tau_{\max}$.

Taking into account the limitations related to BA, SD, and DTL, as well as considering the functional relationship between the anti-interference coefficient and H_∞ robust performance in gaming, an anti-interference coefficient of $\gamma = 12.5$ is chosen. The cone complement linearization iterative algorithm and dichotomy method are utilized to determine the critical delay $\tau_{\max} = 29.2$ ms.

4. Response delay analysis

The approach to solving the gain of the delay-dependent H_∞ robust controller is to pre-set the system response delay and the anti-interference coefficient. If the system is in a state of instability ($\tau_{act} > \tau_{\max}$), it is not possible to obtain the feedback gain of the H_∞ delay-dependent robust controller [23]. To verify the feasibility of the proposed control method, this paper tests the true actuator response delay. Literature [23] introduces the concept of response delay for an MR damper, which is defined as the time required for the system to transition from one stable state to another, encompassing 63.2% of the total transition time when there are changes in the system state. Since determining the response delay of an MR damper involves considering the interaction between both the response time of electromagnetic loop and the time required to establish a control force, theoretical analysis alone cannot clearly distinguish specific stages at which these occur. Therefore, overall response delay can only be determined through experiment. To this end, an open-loop control system for an MR damper comprising components such as a current driver, current sensor, oscilloscope, power supply and signal generator is first established as shown in Fig. 3a.

The purpose here is mainly testing the response time within electromagnetic loops related to an MR damper. Specifically, the current driver transmits separate current signals to the MR damper, and the response is measured by the current sensor. The electromagnetic response time of different input currents is then calculated. The specific flow of the closed-loop control experiment is shown in Fig. 3c, and the test results are displayed in Fig. 4a. It is evident that the open-loop response time T_u of the upper step (current loading) ranges from 40 to 50 ms, while the open-loop response time T_d of the lower step (current cut-off) ranges from 38 to 43 ms. It can be seen that as the input current increases, the response time decreases. However, both the

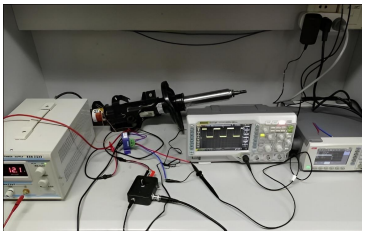

(a) Open-loop system

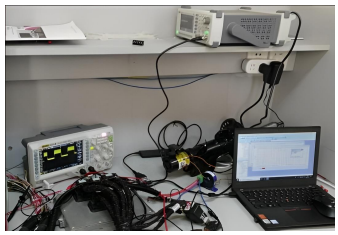

(b) closed-loop system

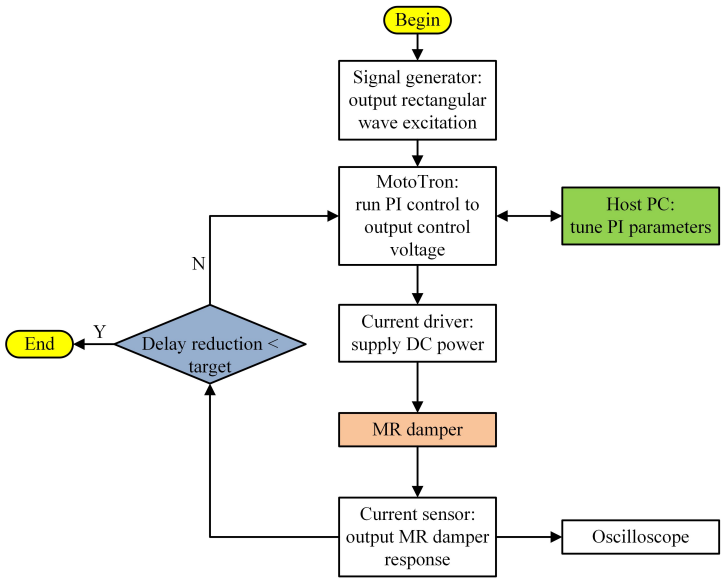

(c) Flow chart of the closed-loop control experiment.

Fig. 3. Control system of MR damper.

load time and cut-off time exceed the theoretical critical delay limits. When factoring in the setup time needed for the control force, it becomes clear that the actual response delay will surpass the system's allowed theoretical critical delay for maintaining stability.

A PI control method has been developed to minimize response delay, as shown in Fig. 3b. In comparison with the open-loop control system, both an upper computer and a MotoTron system have been added. The specific test process is as follows: first, the sensor model, PI algorithm, and output model are constructed in the upper computer and then compiled and downloaded into the MotoTron system. Next, a signal generator outputs the test condition to the MotoTron system. The MotoTron system operates the PI algorithm and outputs a target control voltage (i.e., PWM signal) to the current driver, and subsequently, the driver inputs this target current to the MR damper. Feedback on the actual current signal is provided by a series-connected current sensor in order to enable closed-loop PI control of the driving current within the circuit operation. The power supply is utilized to provide power to the MotoTron system and current drivers. The oscilloscope is used to display the real-time current response of the drive, while the upper computer is employed for recording data. The response characteristics using a PI control algorithm are depicted in Fig. 4b. It is evident that the response time of both upper and lower steps of the MR damper with a PI control algorithm can be controlled within 16ms. Based on this result, a triangular wave excitation

test is conducted following the approach outlined in [23], with the test arrangement mirroring which is illustrated in Fig. 1. The overall response time is determined based on sampling points during both on- and off-excitation currents. The global response delay calculation method for an MR damper is represented by (17).

$$\tau = \frac{n_2 - n_1}{f} \times 62.3‰, \tag{17}$$

where n_1 represents the number of points used at the end of the initial state, n_2 denotes the number of sampling points that reached the stable state, and f stands for the sampling frequency. Given the tendency of the electromagnetic response time for up/down steps beyond 1.6 A of the driving current, this study focuses on measuring the overall response time when the driving current transitions from 0 to 1.6 A, resulting in a value of 27.9 ms. In other words, it is found that the overall actual response time is lower than the theoretical critical delay allowed by the system to maintain stability.

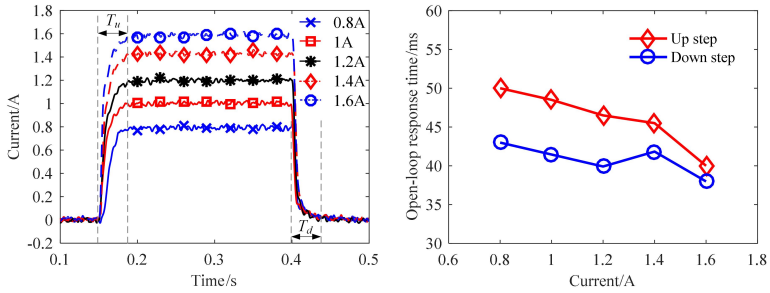

(a) Open-loop control system.

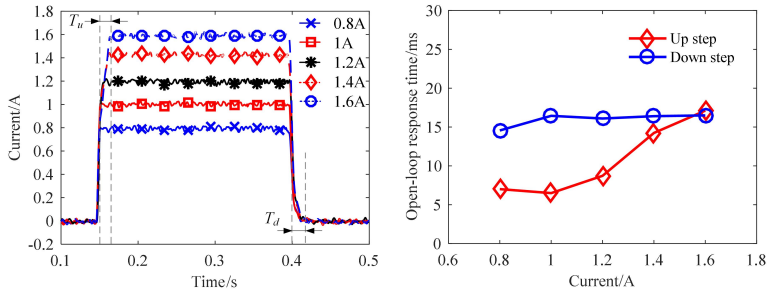

(b) Closed-loop control system.

Fig. 4. Electromagnetic response time.

According to the test results, the feasible solution (feedback gain) of the delay-dependent H_∞ controller (Controller I) is $K = 10^4 \times [1.50061.6256 - 0.1557 - 0.0037]$. As a comparison, a delay-independent H_∞ controller (Controller II) is designed, and the controller gain is $K = 10^4 \times [2.1345 - 0.0122 - 0.0011 - 0.085]$.

5. Simulation results

To validate the efficacy of Controller I, a comparison was made between the system's dynamic performance on bumpy and random roads with that of passive suspension and Controller II. The relevant simulations are conducted. The excitation of a random road can be mathematically found as:

$$\dot{z}_r(t) = -\omega_0 z_r(t) + 2\pi n_0 \sqrt{G_q(n_0)v} \cdot \omega(t)', \tag{18}$$

where $\omega_0 = 2\pi f_0$ denotes the cut-off angle frequency, and $f_0 = 0.01$ represents the cut-off frequency; $\omega(t)$ represents the white noise signal, $z_r(t)$ represents the road profile, v represents the driving speed, $G_q(n_0)$ denotes the road roughness coefficient.

The bump excitation is:

$$z_r = \begin{cases} 0.05 \cdot \left(1 - \cos \frac{2\pi v}{L} \cdot t\right), & 0.5 \text{ s} < t < 1 \text{ s} \\ 0, \text{ another} \end{cases}, \tag{19}$$

where v represents the vehicle speed and $v = 10$ m/s is the one selected here, L represents the length of the bump and $L = 5$ m is selected.

5.1. Bumpy road

Figure 5 illustrates the dynamic performance ($\tau_{act} = 27.9$ ms). Table 1 presents a comparison of the peak-to-peak responses. It is evident that, in comparison to passive control, controllers I and II exhibit significantly reduced peak-to-peak responses to each performance index. Specifically, in comparison to passive control, the former is reduced by 24.6%, 13.8%, and 7.7%, while the latter decreased by 19.7%, 11.3%, and 15.4% respectively.

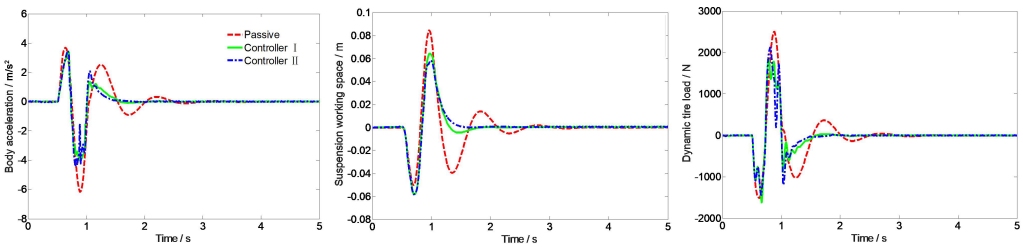

Fig. 5. Dynamic performance comparison.

Table 1. Peak-to-peak response comparison.

Index	BA (m/s^2)			SD (m)			DTL (N)		
	Passive	Controller I	Controller II	Passive	Controller I	Controller II	Passive	Controller I	Controller II
Peak-to-Peak	9.85	7.43	7.91	0.13	0.12	0.11	4009	3454	3556
Improvement	–	↓ 24.6%	↓ 19.7%	–	↓ 7.7%	↓ 15.4%	–	↓ 13.8%	↓ 11.3%

5.2. Random road

Figure 6 illustrates the comparison of dynamic performance for each control method under C-grade road conditions ($G_q(n_0) = 256\times10^{-6}$ m^{-1}). Table 2, in turn, presents a comparison of each performance index. It is evident that, in comparison to passive control, the improvement of dynamic performance provided by Controller I and Controller II is primarily manifested in vertical BA and SD, with limited impact on road holding. Specifically, Controller I and Controller II exhibit

Metrol. Meas. Syst., Vol. 31 (2024), No. 4, pp. 797–812
DOI: 10.24425/mms.2024.152051

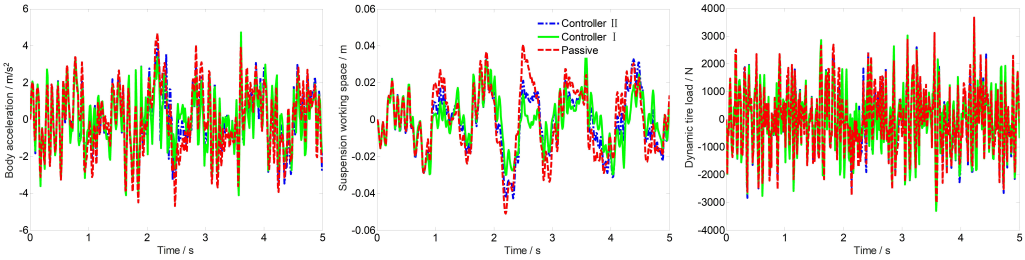

Fig. 6. Dynamic performance comparison.

increases of 19.7% and 13.3% respectively in BA, along with improvements of 30.9% and 16.2% respectively in SD. Furthermore, when compared with Controller II, it can be observed that the BA, SD and DTL decreased by 7.4%, 17.6%, and 1.1% respectively for Controller I.

Table 2. RMS value comparison of dynamic performances.

Controller	BA (m/s^2)	SD (m)	DTL (N)
Passive	1.92	0.021	1166
Controller I	1.54(↓19.7%)	0.014(↓30.9%)	1139(↓2.3%)
Controller II	1.66(↓13.3%)	0.017(↓16.2%)	1151(↓1.3%)

The Fourier transform is employed for analysis of time-domain data in order to obtain the amplitude-frequency characteristics of various performance indicators (Fig. 7). It is evident that, in comparison with passive control, Controller I and Controller II have significantly enhanced the low-frequency formant amplitude of each performance index. However, there is no apparent improvement for the high-frequency formant amplitude, indicating that the response delay primarily affects the first-order main mode (i.e., body vibration) of MR SAS, with less impact on the second-order main vibration mode (i.e., wheel vibration) of MR SAS. This finding aligns with the simulation results under bump road excitation.

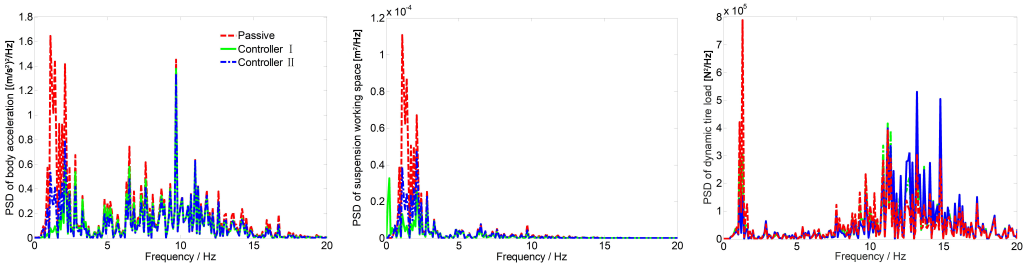

Fig. 7. Amplitude frequency characteristics comparison.

6. Test verification

6.1. Control system design

As shown in Fig. 8a, a quarter McPherson test bench is built for rapid prototyping control tests. The test system (Fig. 8b) mainly includes a controller, MR damper driver, DC power supply, oscilloscope, acceleration sensor, and an INSTRON 8800 CNC hydraulic servo vibration test bench.

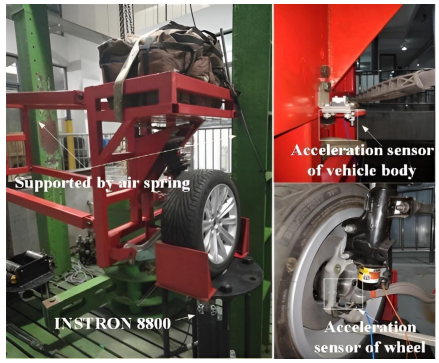

(a) McPherson test bench.

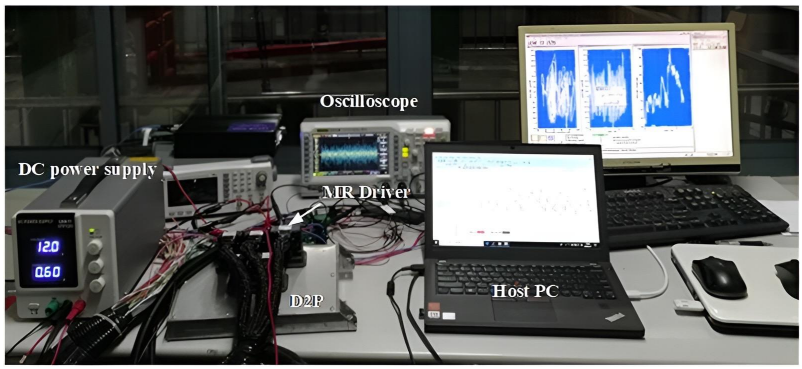

(a) McPherson test bench.

Fig. 8. Test bench.

Since the acceleration sensor is only utilized for measuring the vehicle body and wheel acceleration, the state variables required in (9) cannot be directly obtained. Therefore, it is necessary to integrate the acceleration signal once or twice in order to acquire the absolute velocity and displacement respectively. Given that integration often introduces errors into a signal, a combined filter depicted in Fig. 9 has been designed to process the acceleration signal. The combined filter primarily consists of a first-order low-pass filter $L(s)$, $L_i(s)$ for integrating the acceleration signal, and a first-order high-pass filter $H(s)$.

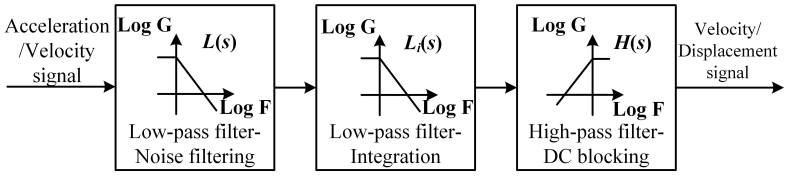

Fig. 9. Combined filter.

Table 3. Cut-off frequency.

Filter	$L(s)$	$L_i(s)$	$H(s)$
Cut-off frequency (Hz)	50	0.1	0.5

6.2. Analysis of test results

Figure 10 illustrates the results of dynamic performance testing for each control method under bump road excitation, with the test input being identical to the simulation input. The peak-to-peak response of the three control methods is presented in Table 4. It is evident that, in comparison to passive control, delay-dependent control (Controller I) demonstrates a reduction of 38.6%, 16.7%, and 14.3% in BA, DTL, and SD respectively. Similarly, delay-independent control (Controller II) shows aecrease of 26.6%, 25%, and 7.3% compared to passive control for these parameters. Moreover, when comparing delay-dependent control (Controller I) with delay independent control (Controller II), it is observed that the peak-to-peak response to vehicle BA and DTL decreases by 16.4% and 7.4% respectively for delay-dependent control. Overall, these results indicate significant improvements in reducing peak-to-peak values for BA, DTL, and SD when utilizing both delay-dependent and delay-independent controls as compared to passive control during bump road excitation testing.

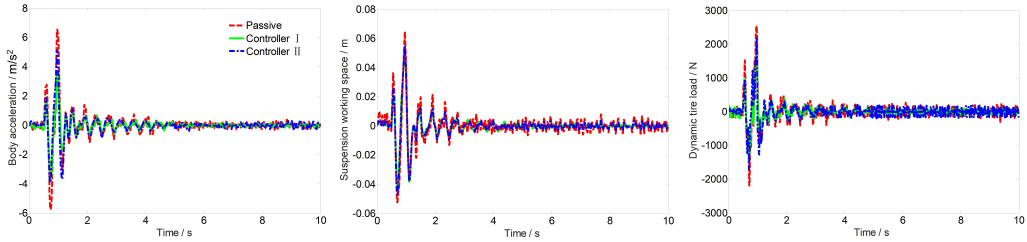

Fig. 10. Dynamic performance test results of different control methods under bump road excitation.

Table 4. Peak-to-peak response of the three control methods.

Index	BA (m/s^2)			SD (m)			DTL (N)		
	Passive	Controller I	Controller II	Passive	Controller I	Controller II	Passive	Controller I	Controller II
Peak-to-Peak	12.29	7.54	9.02	12.29	7.54	9.02	12.29	7.54	9.02
Improvement	–	↓38.6%	↓26.6%	–	↓38.6%	↓26.6%	–	↓38.6%	↓26.6%

It is important to note that the fluctuation of dynamic performance indexes following bump excitation is attributed to the fact that the single-channel test bench is anchored to the ground through an air spring. When the vibration test bench produces pulse excitation, in accordance with the principles of force and reaction force, the entire test bench will vibrate with a specific amplitude. This explains why the acceleration sensor can continue to capture vibration acceleration signals even after the shaking table ceases to output force.

Figure 11 depicts the dynamic performance test results of each control method under random road excitation, with the corresponding performance indices provided in Table 5. It is evident that, when compared to passive control, the enhanced dynamic performance of Controller I and Controller II primarily manifests in reduced vertical BA and SD, while the improvement in road holding is limited, consistent with simulation results. Specifically, in comparison with passive control, both Controller I and Controller II exhibit a decrease of 16.7% and 13.6%, respectively, in BA, as well as reductions of 39.6% and 27.1%, separately, in SD. Moreover, compared to Controller II, a decrease of 3.5% in vertical acceleration, a reduction of 17.1 % in SD and an overall decline by 0.89 % of DTL are observed for Controller I. It should be noted that the overall trend of amplitude-frequency characteristics for each performance index, aligns with the simulation results. Therefore, further elaboration on this matter will not be provided here.

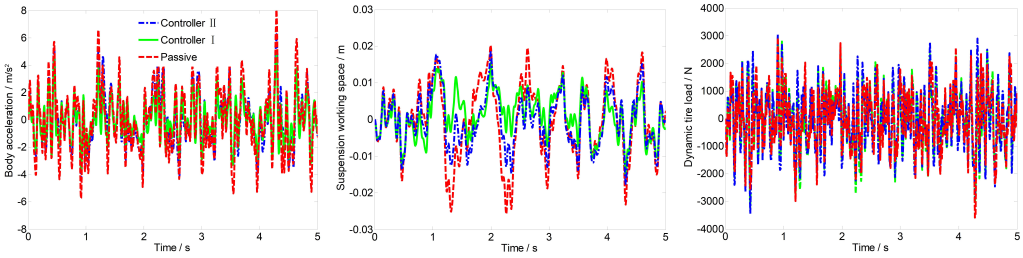

Fig. 11. Dynamic performance test results.

Table 5. RMS values of each performance index.

Controller	BA(m/s^2)	SD (m)	DTL (N)
Passive	1.98	0.0096	1156
Controller I	1.65(↓16.7%)	0.0058(↓39.6%)	1110(↓3.97%)
Controller II	1.71(↓13.6%)	0.007(↓27.1%)	1120(↓3.11%)

The test results also confirm the efficacy of the proposed control method, with overall trends consistent with the simulation results. However, some discrepancies exist between the simulation and test results, which are shown in Tables 6 and 7. Taking Controller I as an example, compared to the simulation results, the BA in the test data is larger, while SD and DTL are decreased. This discrepancy can be attributed to the use of a linear suspension model in the simulation analysis versus a McPherson suspension system with structural nonlinearity in the test verification. In addition to the damping force generated by the MR damper, friction effects between components also contribute to damping force during testing, resulting in greater actual damping than indicated by simulation analysis. While increased damping is advantageous for reducing SD and DTL, it concurrently leads to higher BA during testing.

Table 6. Comparison between simulation and test for bump pavement.

	Peak-to-peak value of BA (m/s^2)	Peak-to-peak value of SD (m)	Peak-to-peak value of DTL (N)
Simulation	7.43	0.12	3454
Test	7.54	0.1	3306

Table 7. Comparison between simulation and test for random road.

	BA (m/s^2)	SD (m)	DTL (N)
Simulation	1.54	0.014	1139
Test	1.65	0.0058	1110

7. Conclusions

This paper presents the design of a time-delay dependent H_∞ robust controller for MR SAS. To address the association between the actual response delay and the theoretical critical delay of the designed delay-dependent controller, a PI control algorithm is developed. The main findings can be summarized as follows:

1. The simulation results suggest that, in comparison with the delay-independentH_∞ robust controller, the peak-to-peak response of BA and DTL is reduced by 6.1% and 2.9% respectively under bump road conditions, with minimal impact on road holding. When compared to the time delay-independent H_∞ robust control, the vehicle body vertical acceleration, SD, and DTL are reduced by 7.4%, 17.6%, and 1.1% respectively under random road conditions.
2. The test results indicate that, in comparison with the delay-independent H_∞ robust controller, the peak-to-peak response of vehicle BA and DTL is reduced by 16.4% and 7.4% respectively under bump road conditions, with little change in road holding. When compared to the delay-independent H_∞ robust control, the BA, SD, and DTL are decreased by 3.5%, 17.1%, and 0.89% respectively under stochastic road conditions.

In the future, further research will be conducted on semi-active suspension control considering system uncertainty, building upon the findings of this paper. Additionally, future research will also take into account the entire vehicle model in order to better align with engineering practice.

Acknowledgements

The author(s) disclosed receipt of the following financial support for the research, authorship, and/or publication of this article: The present work is supported by the Open Fund of State Key Laboratory of Automotive Simulation and Control (Project Number-20210204)

References

[1] Ding, R., Wang, R., Meng, X., Liu, W., & Chen, L. (2021). Intelligent switching control of hybrid electromagnetic active suspension based on road identification. *Mechanical Systems and Signal Processing*, *152*, 107355. https://doi.org/10.1016/j.ymssp.2020.107355

[2] Sun, X., Wu, M., Yin, C., Wang, S., & Tian, X. (2021). Multiple-Iteration Search Sensorless Control for Linear Motor in Vehicle Regenerative Suspension. *IEEE Transactions on Transportation Electrification*, *7*(3), 1628–1637. https://doi.org/10.1109/tte.2021.3052989

[3] Chen, L., Ding, R., Meng, X., & Wang, R. (2023). Optimal design and experimental research on a new HEMA with energy reduction for vehicle suspension systems. *International Journal of Vehicle Design*, *93*(1/2), 66–86. https://doi.org/10.1504/ijvd.2023.10060273

[4] Liu, W., Wang, R., Ding, R., Meng, X., & Yang, L. (2020). On-line estimation of road profile in semi-active suspension based on unsprung mass acceleration. *Mechanical Systems and Signal Processing*, *135*, 106370. https://doi.org/10.1016/j.ymssp.2019.106370

[5] Cha, Y.-J., Agrawal, A. K., & Dyke, S. J. (2012). Time delay effects on large-scale MR damper based semi-active control strategies. *Smart Materials and Structures*, *22*(1), 015011. https://doi.org/10.1088/0964-1726/22/1/015011

[6] Yoon, D.-S., Park, Y.-J., & Choi, S.-B. (2019). An eddy current effect on the response time of a magnetorheological damper: Analysis and experimental validation. *Mechanical Systems and Signal Processing*, *127*, 136–158. https://doi.org/10.1016/j.ymssp.2019.02.058

[7] Pang, H., Fu, W.-Q., & Liu, K. (2015). Stability analysis and fuzzy Smith compensation control for semi-active suspension systems with time delay. *Journal of Intelligent & Fuzzy Systems*, *29*(6), 2513–2525. https://doi.org/10.3233/ifs-151954

[8] Tao, L., Chen, S., Fang, G., & Zu, G. (2019). Smith Predictor-Taylor Series-Based LQG Control for Time Delay Compensation of Vehicle Semiactive Suspension. *Shock and Vibration*, *2019*(1). https://doi.org/10.1155/2019/3476826

[9] Li, G., Gan, Y., Liu, Q., Xu, H., Chen, D., Zhong, L., Deng, J., & Hu, G. (2024). Performance analysis of vehicle magnetorheological semi-active air suspension based on S-QFSMC control. *Frontiers in Materials*, *11*. https://doi.org/10.3389/fmats.2024.1358319

[10] Karim Afshar, K., Javadi, A., & Jahed-Motlagh, M. R. (2018). Robust control of an active suspension system with actuator time delay by predictor feedback. *IET Control Theory & Applications*, *12*(7), 1012–1023. https://doi.org/10.1049/iet-cta.2017.0970

[11] Gu, B., Cong, J., Zhao, J., Chen, H., & Fatemi Golshan, M. (2022). A novel robust finite time control approach for a nonlinear disturbed quarter-vehicle suspension system with time delay actuation. *Automatika*, *63*(4), 627–639. https://doi.org/10.1080/00051144.2022.2059205

[12] Yin, Y., Luo, B., Ren, H., Fang, Q., & Zhang, C. (2022). Robust control design for active suspension system with uncertain dynamics and actuator time delay. *Journal of Mechanical Science and Technology*, *36*(12), 6319–6327. https://doi.org/10.1007/s12206-022-1143-1

[13] Li, J. W., Luo, J. N., Huang, Z. (2024). Study on a semi-active suspension controller considering time delay of CDC system. *Vehicle Engineering*, 46(05), 913–922. https://doi.org/10.19562/j.chinasae.qcgc.2024.05.017

[14] Yang, L. Q., Zhao, Y. Y. (2023). Multi-objective optimization design of a grounded stiffness time delay feedback dynamic vibration absorber with inerter. *Journal of Vibration and Shock*, *42*(23), 133–143.

[15] Liu, C., Chen, L., Zhang, X., & Yang, X. (2020). Stability analysis of semi-active inerter-spring-damper suspensions based on time-delay. *Journal of Theoretical and Applied Mechanics*, *58*(3), 599–610. https://doi.org/10.15632/jtam-pl/121975

[16] Wu, K., Ren, C., & Atay, F.M. (2024). Enhancing energy recovery in automotive suspension systems by utilizing time-delay. *Energy*, *300*, 131578. https://doi.org/10.1016/j.energy.2024.131578

[17] Zhu, M., Lv, G., Zhang, C., Jiang, J., & Wang, H. (2022). Delay-Dependent Sliding Mode Variable Structure Control of Vehicle Magneto-Rheological Semi-Active Suspension. *IEEE Access*, *10*, 51128–51141. https://doi.org/10.1109/access.2022.3173605

[18] Nan, Y., Shao, S., Ren, C., Wu, K., Cheng, Y., & Zhou, P. (2023). Simulation and Experimental Research on Active Suspension System with Time-Delay Feedback Control. *IEEE Access*, *11*, 88498–88510. https://doi.org/10.1109/access.2023.3305265

[19] Hong, S. R., Wereley, N. M., Choi, Y.T., & Choi, S. B. (2008). Analytical and experimental validation of a nondimensional Bingham model for mixed-mode magnetorheological dampers. *Journal of Sound and Vibration*, *312*(3), 399–417. https://doi.org/10.1016/j.jsv.2007.07.087

[20] Ding, R., Wang, R., Meng, X., & Chen, L. (2019). Energy consumption sensitivity analysis and energy-reduction control of hybrid electromagnetic active suspension. *Mechanical Systems and Signal Processing*, *134*, 106301. https://doi.org/10.1016/j.ymssp.2019.106301

[21] El Ghaoui, L., Oustry, F., & AitRami, M. (1997). A cone complementarity linearization algorithm for static output-feedback and related problems. *IEEE Transactions on Automatic Control*, *42*(8), 1171–1176. https://doi.org/10.1109/9.618250

[22] Gouaisbaut, F., & Peaucelle, D. (2006). Delay-dependent stability analysis of linear time delay systems. *IFAC Proceedings Volumes*, *39*(10), 54–59. https://doi.org/10.3182/20060710-3-it-4901.00010

[23] Koo, J.-H., Goncalves, F.D., & Ahmadian, M. (2004). Investigation of the response time of magnetorheological fluid dampers. In K.-W. Wang (Ed.), *SPIE Proceedings* (Vol. 5386, p. 63). SPIE. https://doi.org/10.1117/12.539643